LBL-27116 c.2

Lawrence Berkeley Laboratory
UNIVERSITY OF CALIFORNIA

Presented at the Symposium on Nuclear Dynamics and Nuclear Disassembly, Dallas, TX, April 10–14, 1989, and to be published in the Proceedings

Excitation and Multiple Dissociation of Projectiles at Intermediate Energy

DEC 1 1 1 0 0

J. Pouliot, Y. Chan, A. Dacal, D.E. DiGregorio, B.A. Harmon, R. Knop, M.E. Ortiz, E. Plagnol, R.G. Stokstad, C. Moisan, L. Potvin, C. Rioux, and R. Roy

April 1989

NUCLEAR SCIENCE DIVISION

LBL-27116 c.2

Prepared for the U.S. Department of Energy under Contract Number DE-AC03-76SF00098.

DISCLAIMER

This document was prepared as an account of work sponsored by the United States Government. While this document is believed to contain correct information, neither the United States Government nor any agency thereof, nor the Regents of the University of California, nor any of their employees, makes any warranty, express or implied, or assumes any legal responsibility for the accuracy, completeness, or usefulness of any information, apparatus, product, or process disclosed, or represents that its use would not infringe privately owned rights. Reference herein to any specific commercial product, process, or service by its trade name, trademark, manufacturer, or otherwise, does not necessarily constitute or imply its endorsement, recommendation, or favoring by the United States Government or any agency thereof, or the Regents of the University of California. The views and opinions of authors expressed herein do not necessarily state or reflect those of the United States Government or any agency thereof or the Regents of the University of California.

Excitation and Multiple Dissociation of Projectiles at Intermediate Energy.

J.Pouliot, Y.Chan, A.Dacal, D.E.DiGregorio, B.A.Harmon, R.Knop , M.E.Ortiz, E.Plagnol and R.G.Stokstad

Nuclear Science Division, Lawrence Berkeley Laboratory, 1 Cyclotron Road, Berkeley, CA 94720

and

C.Moisan, L.Potvin, C.Rioux and R.Roy

Laboratoire de Physique Nucléaire, Université Laval, Québec, G1K 7P4, Canada

April 1989

Invited talk prepared for presentation at the Symposium on Nuclear Dynamics and Nuclear disassembly, Dallas, Texas, 10-14 April 1989. To be published in the Conference Proceedings by World Scientific Publishing Co. Inc., Teaneck, NJ 07666.

Excitation and Multiple Dissociation of Projectiles at Intermediate Energy.

J.Pouliot, Y.Chan, A.Dacal†, D.E.DiGregorio*, B.A.Harmon, R.Knop , M.E.Ortiz†, E.Plagnol and R.G.Stokstad**

Nuclear Science Division, Lawrence Berkeley Laboratory, 1 Cyclotron Road, Berkeley, CA 94720

and

C.Moisan††, L.Potvin, C.Rioux and R.Roy

Laboratoire de Physique Nucléaire, Université Laval, Québec, G1K 7P4, Canada

ABSTRACT

Cross sections for the multiple breakup of ^{16}O, ^{14}N and ^{12}C projectiles scattered by a Au target were measured with an array of 34 phoswich detectors. The dissociation of the projectiles into as many as five charged particles has been observed. The yields of different exit channels correlate approximately with the threshold energy for separation of the projectile into the observed fragments. The excitation spectrum of the primary projectile-like nucleus was reconstructed from the measured positions and kinetic energies of the individual fragments. The energy sharing between projectile and target is consistent with a fast excitation mechanism in which differential increases in projectile excitation energy appear to be accompanied by comparable increases in target excitation. Calculations of the yields based on a sequence of binary decays are presented. The question of prompt or sequential decay is also considered by examining the directional correlations of the particles.

1. INTRODUCTION

The investigation of heavy ion reactions in the intermediate energy domain (20 to 100 MeV/A) has received a lot of attention in the last decade. This is partly because new accelerators capable of covering this domain have come into operation, but mainly because the first experiments have shown features pertinent to both low and high energy domains[1)], implying that this intermediate region would be a transition zone. The study of the breakup

Permanent addresses:

†Instituto de Física, UNAM, México D.F. 01000, México.

* Departamento de Física-TANDAR, CNEA, 1429 Buenos Aires, Argentina and CONICET.

** GANIL BP 5027 F-14021 Caen CEDEX France.

†† Foster Rad. Lab., Université McGill, Montréal, Québec, Canada H3A 2B2.

of a projectile into its component fragments generally has been based either on the inclusive detection of a single fragment or on two-particle coincidence measurements[2]. These types of experiments can reveal much about the breakup process when the two-body exit channels are dominant[3,4]. It is well known, however, that the average number of particles produced in a heavy ion collision increases rapidly with bombarding energy in the intermediate energy region. A large multiplicity and many different exit channels can result from the multiple breakup of the projectile in peripheral interactions with the target. When this is the case, it is difficult or impossible to obtain a detailed understanding of the reaction process through inclusive or two particle coincidence measurements. The goal of this experiment, therefore, was to observe all or most of the projectile breakup products with a multi-element array and to determine the extent of multiple dissociation.

In this paper, we describe a study of the reactions of ^{16}O, ^{14}N and ^{12}C on a gold target at 32.5 MeV/A. After a brief description of the experimental setup and the analysis procedure, we present the measurements of the cross sections for the dissociation of the projectile into its constituent particles. The excitation energy of the projectile-like nucleus is then reconstructed. Within the assumption of a primary two-body process, the excitation energy sharing between the target and the projectile is obtained. The question of prompt versus sequential decay is then addressed: this is done by comparing sequential binary decay calculations with the experimental yields and by comparing calculated and measured directional correlations for the breakup of ^{16}O into four alpha particles.

2. EXPERIMENT AND DATA ANALYSIS

The experiment was performed at the 88-Inch Cyclotron of the Lawrence Berkeley Laboratory. Beams of fully-stripped ^{16}O, ^{14}N, and ^{12}C ions were produced in an Electron Cyclotron Resonance ion source and accelerated to an energy of 32.5 MeV/nucleon. Beam intensities were kept low (a few tenths of an electrical nanoampere) because of the high counting rates seen by the detectors closest to the beam. The self-supporting gold target was 2 mg/cm^2 thick.

2.1 Detection System

We have constructed an array of 34 fast/slow plastic phoswich detectors[5]. Each element has the shape of a truncated pyramid (Fig.1.), which permits close packing. The

front edge of a single element is 17 mm long and subtends an angle of 5°. An element consists of a 1mm thick fast scintillator (2 ns decay time) followed by 102 mm of a slow scintillator (225 ns). A photomultiplier tube is glued directly to the back of the slow plastic. Because each detector is tapered and views the target directly, the effective solid angle is independent of the particle range. Particles are identified by separately integrating the analog signal by a short and a long time gate. Protons and deuterons, and elements up to the charge of the projectile, could be resolved. The geometry of the array for a 7x7 (horizontal x vertical) configuration is illustrated in Fig.1. A 5x7 configuration, centered on the beam axis, was used in the present experiment. Three vertical strips of position sensitive plastic scintillator[6] were mounted on each side of the array to extend the angular coverage out to ±35°. All coincidences between three or more particles were recorded, while those involving only two particles were scaled down by a factor of 128. Random coincidences were negligible.

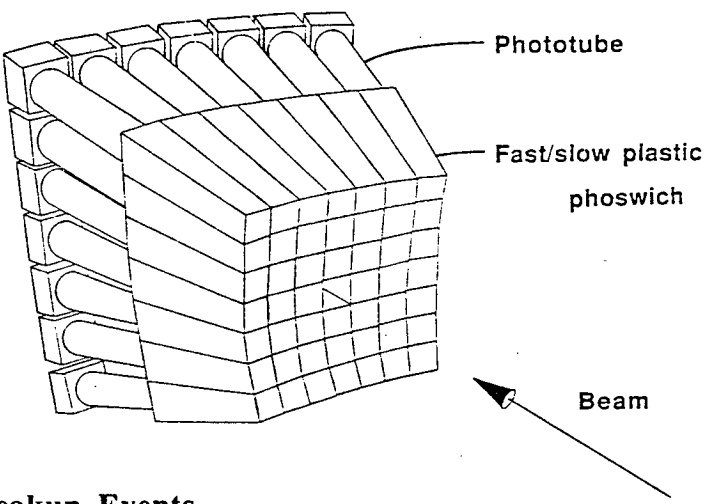

Fig. 1. Perspective view of the array. The detectors are configured in a 7 x 7 configuration. The center is left open to allow the beam to go through the array when placed at 0°.

2.2 Selecting Projectile Breakup Events

Events resulting from the breakup of the primary projectile-like nucleus were selected in the analysis by requiring that the sum of the identified charges be equal to the charge of the projectile. The energy threshold for particle identification of the 1 mm thick fast plastic, effectively eliminated any contributions of low energy particles (with $Z \geq 2$) evaporated by an excited target-like nucleus. The peripheral nature of the reaction was verified by observing that the velocities of all the detected fragments, including protons, were characteristic of the projectile and that the velocity, V_{pp}, of the projectile-like center of mass system of the detected fragments was close to the beam velocity (see Fig.2).

The peripheral nature of the reaction was also checked by observing that the relative yields of different channels were approximately independent of the target. This feature was demonstrated by making additional measurements on targets of ^{12}C and ^{9}Be[7].

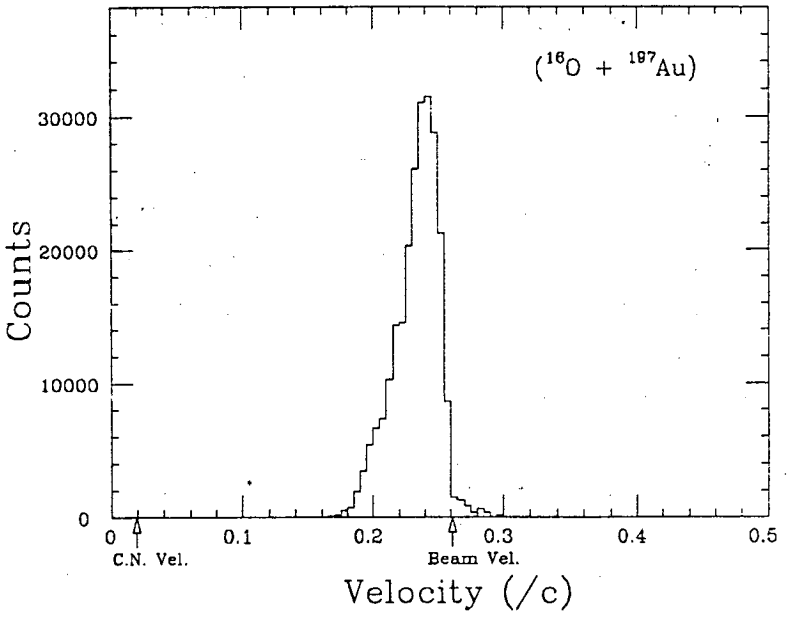

Fig. 2. The velocity of the center of mass system V_{pp} is obtained from the sum of the momentum of each fragment (with charge Z_i) divided by the mass of the projectile. To be included, an event must fulfill the condition $\Sigma_i Z_i = Z_{proj}$. Breakup channels ($M \geq 2$) are shown. Beam velocity and compound nucleus velocity are indicated by the arrows.

2.3 Efficiency

The close packing of the detectors in the array produces a high efficiency for incident particles. However, even for forward peaked projectile breakup reactions, it is possible for one or more fragments to miss the array. The efficiency of the array for detecting a given breakup channel was first determined empirically. The probability of detecting a particular particle in a given channel was estimated by extrapolating the observed angular distribution for that particle into the regions not covered by the array. In this way, alpha particles were found to have similar angular distributions for all channels. Thus, the angular distribution of alpha particles in the C+He channel was almost the same as in the He+He+He+He channel. This suggests that the correlations among the particles in a given channel can be neglected in determining the efficiency of the array and that the efficiency is approximated by the product of the probabilities for detecting individually each of the fragments making up that channel. For example, the overall detection efficiencies, for the two-body channel C+He and the four-body channel Li+He+He+H, were estimated to be 67% and 32%, respectively. This procedure was checked for the two-body channels

by comparing the number of light particles observed in the vertical strips with the expectation based on the extrapolation of the angular distributions measured with the array.

Efficiencies were also determined theoretically by simulating the sequential decay of an equilibrated projectile with the Monte Carlo code LILITA[8]. The simulation included the geometry of the array (the center hole and and all individual detectors) as well as the energy thresholds. This study showed that the effects of correlations were small and that double hits (two particles hitting the same detector element), with the exception of alpha particles generated by the decay of ^{8}Be(g.s.), could be neglected. The empirical efficiencies were well reproduced for those channels in which all fragments had masses equal to or greater than 4. The theoretical efficiencies for channels containing hydrogen isotopes, however, were too small because the protons were predicted to have broader angular distributions than observed. The use of empirical efficiencies, instead of the theoretical efficiencies discussed above, reduces the dependence of the deduced cross sections on the choice of a model for the reaction.

3. RESULTS

3.1 Channel Cross Sections

The deduced cross sections of the different channels for each of the three beams (^{16}O, ^{14}N and ^{12}C) are plotted in Fig. 3 as a function of the separation energy (Q_o) for that channel. The channels and their Q_o values are given in the table adjacent to the figure. The absolute normalization (corrected for efficiency) was established by comparison of the measured elastic scattering to the Rutherford cross section and also by comparing the inclusive yields of heavy ions to those measured with a solid-state detector in an earlier experiment[9]. The two determinations were in good agreement; the systematic error on the absolute normalization was estimated to be ±20%.

The channels shown in Fig. 3 are distinguished experimentally only by their combination of atomic numbers. For example the contributions of ^{12}B+^{3}He+p and ^{10}B+^{4}He+d are summed together and are plotted against the most positive Q_o value or −23.1 MeV. The detection of ^{8}Be poses an additional complication in that there is a 60% probability that the two ^{4}He nuclei from the decay of a ^{8}Be(g.s.) nucleus will hit the same detector. Such double hits were identified as Z=4 and were not distinguished from ^{7,9}Be.

Therefore, we have summed all events which differed only by two Z=2 fragments or one Z=4 fragment (such as 4*He, 2*He+Be, and Be+Be) and plotted them versus the most positive Q_0 value. These channels are indicated by an arrow in Fig. 3.

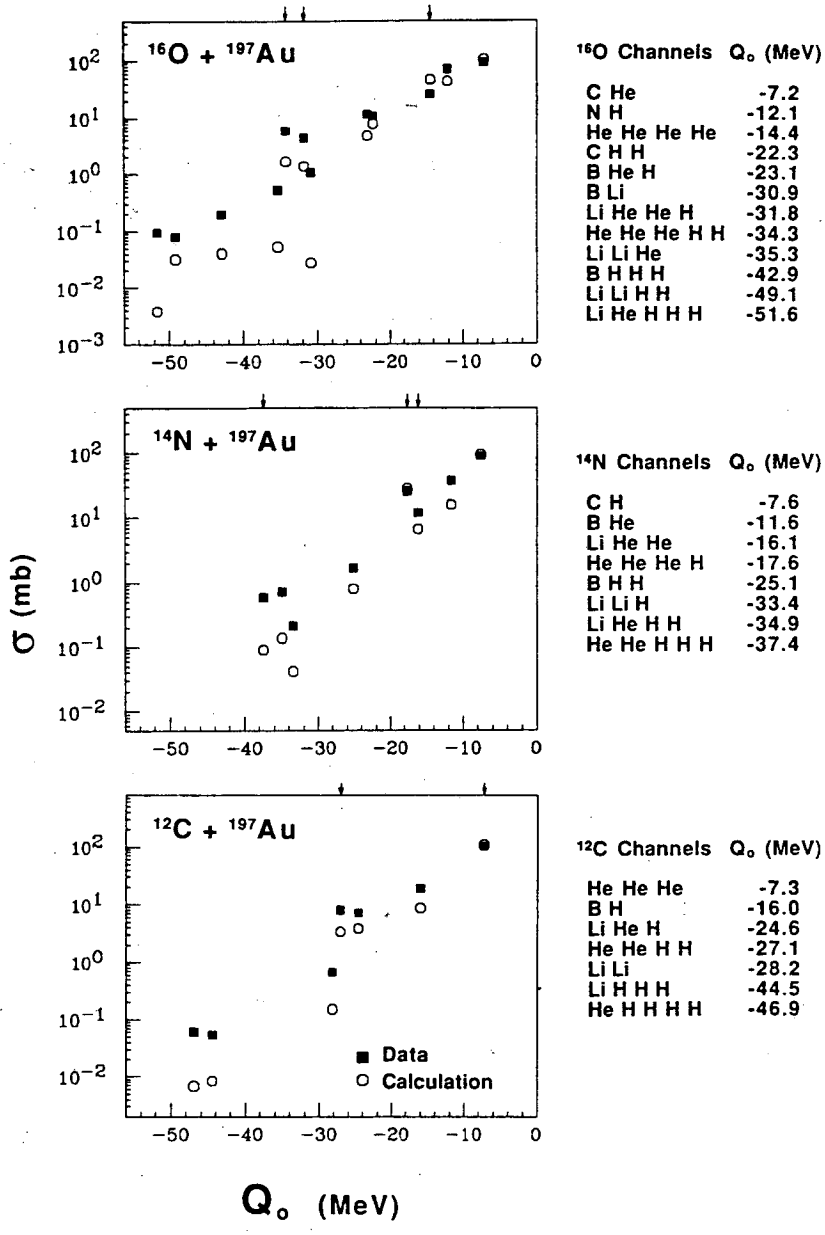

Fig. 3. Cross section of breakup channels plotted versus the most positive Q_0 value of all isotopic combinations consistent with the elements making up that channel. The channels containing a combination of two helium nuclei or a Be nucleus have been summed and are indicated by an arrow. The open circles show the results of a statistical decay calculation[10] (see Section 4.)

The logarithm of the cross section (Fig. 3) has an approximately linear relationship with Q_o over a range of 3 to 4 orders of magnitude in yield. (The correlation with Q_o value is much stronger than any correlation with particle multiplicity.) Cross sections for breakup can be characterized approximately by a slope parameter, E_o, which has values of 6.4, 5.5 and 6.0 MeV (±0.4) for ^{16}O, ^{14}N, and ^{12}C, respectively. This exponential dependence provides the justification for plotting the cross sections against the most positive Q_o value.

3.2 Excitation Energy of the Projectile-Like Nucleus

The excitation energy spectrum of the primary projectile-like nucleus prior to its decay can be reconstructed from the positions and energies of each of the detected particles under the assumption that the particles originate in the projectile. The total relative kinetic energy of the fragments in the center of mass system of the primary projectile-like nucleus is given by

$$K_{rel} = 1/2 \, \Sigma_i \; m_i \, (V_i - V_{pp})^2 \qquad (1)$$

where V_i is the laboratory velocity of a fragment (with mass m_i). The velocity of the projectile-like center of mass system V_{pp} is obtained from all the fragments with $V_{pp} = 1/M_p \, \Sigma P_i$, and M_p the mass of the projectile. The excitation energy of the primary projectile-like nucleus is:

$$E^*_{pp} = K_{rel} - Q_o \qquad (2)$$

where Q_o is the appropriate Q value for that breakup channel. Residual excitation energies of bound fragments are neglected. The exact position of a recorded particle was chosen at random over the face of the detector. A correction has been made for the different isotopic compositions of a given channel by estimating the yields of each isotopic combination using the above slope parameter and a weighting factor based on $\exp(Q_o/E_o)$. The weighted fraction of events were then offset by the more negative Q_o value associated with that isotopic combination. Figure 4 shows the resulting primary excitation spectrum for ^{16}O. Contributions from some individual channels are also shown.

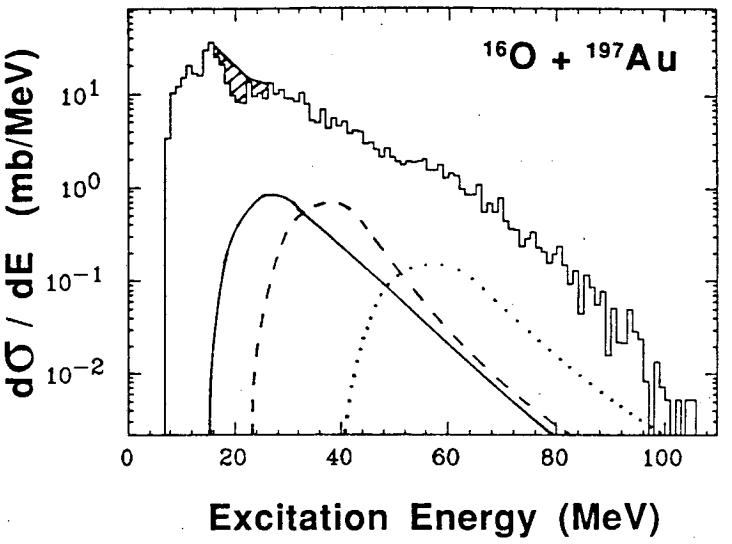

Fig.4. The excitation energy spectrum of the primary projectile-like nucleus for the system $^{16}O+^{197}Au$. The solid, dashed and dotted lines represent contributions of the channels He+He+He+He, C+H+H and He+He+He+H+H respectively. The hatched area represents the estimated contribution of the undetected channel ^{15}O+n. The spectra for the other projectiles were qualitatively similar.

The breakup of the projectile into a channel containing only one charged particle and one or more neutrons will not be included in this spectrum because of the trigger requirement that there be at least a double coincidence. The detectors of course are insensitive to free neutrons. For instance, the contribution of the undetected channel, ^{15}O + n, was estimated by taking the shape of the excitation spectrum from that of N+H, normalizing the total yield according to the empirical dependence on Q_o, and shifting the spectrum by the difference in the Q_o and Coulomb barrier values. The estimated additional contribution of this channel is indicated by the hatched area in Fig.4. Neutrons may also be picked up by the projectile. The pickup reaction $^{197}Au(^{16}O,^{17}O^*)$ has been studied recently by Gazes et al. and shown to populate the channels $^{13}C+^{4}He$ and $^{12}C+^{4}He+n$[11]. Both of these channels are included in the experimental data for which $\Sigma Z=8$. Pickup reactions are also known to produce a generally higher excitation energy in the projectile-like nucleus than does inelastic scattering[12]. We have simulated this process and found that even a level of neutron pickup equal to the intensity of the inelastic scattering does not reproduce the experimental yields for channels with very negative Q_o values. Thus it appears that neutron pickup is at most a partial explanation for the events corresponding to high projectile excitation energies.

There are also reaction mechanisms that may contribute to projectile breakup but that do not strictly satisfy the assumption that all of the detected fragments result solely from the decay of the projectile. Pre-equilibrium emission of protons from the region of overlap between projectile and target is an example of this and might be responsible for the

observed forward-peaked angular correlation of the protons relative to the expectation for sequential decay. Also, final state interactions between fragments of the projectile and the target can alter the directions of the fragments and thereby change the relative kinetic energy and deduced excitation energy[13]. Final state interactions do not affect that portion of the projectile excitation energy associated with the Q_o value for that channel, however.

3.3 Excitation Energy Sharing

The allocation of excitation energy between the projectile and the target is an indication of the degree of thermal equilibrium reached[14]. When the interaction time is long enough to reach thermal equilibrium between the target and the projectile, the total excitation energy is shared according to the ratio of their masses. On the other hand, in a fast process involving collisions of nucleons in the projectile with those in the target, the excitation energy will be shared equally, on average, between projectile and target. The latter is what one would expect for peripheral collisions at intermediate and high energies.

In the preceding section, we deduced the excitation energy of the projectile. The same assumptions allow us to deduce the excitation energy of the target-like nucleus as well. It is given by

$$E^*_T = E_{Beam} - K_{pp} - K_T - E^*_{pp} \tag{3}$$

where K_{pp} is the kinetic energy of the primary projectile-like nucleus obtained from $\mathbf{V}_{pp}$ and K_T is the target-like nucleus kinetic energy evaluated conservation of momentum,

$$\mathbf{P}_{Beam} = \mathbf{P}_T + \mathbf{P}_{pp} \tag{4}$$

where $\mathbf{P}_{Beam}$, $\mathbf{P}_T$ and $\mathbf{P}_{pp}$ are respectively the momentum of the beam, the recoiling target-like nucleus and the projectile-like nucleus. The result of this event by event calculation is shown in Fig. 5. This figure shows the excitation energy correlation between the target-like and the projectile-like nucleus. The tilted solid line on the left indicates the limit of a fully damped reaction where the target and the projectile had sufficient time during the interaction to reach thermal equilibrium. If the parameters $\boldsymbol{d}$, used to calculate the level density parameter $\boldsymbol{a}=A/\boldsymbol{d}$, are the same for the target-like and the projectile-like nucleus, then the relation $E^* = \boldsymbol{a}T^2$ results in an energy sharing corresponding to their mass ratio[14]. Note that very high excitation energies cannot be reached in the projectile in this case because the mass asymmetry favors the target by 12:1.

The other limit represents an equal sharing of energy associated with a fast projectile-target interaction. For instance, a bidirectional exchange of one or more nucleons would result in such a sharing. The contour lines show the results of the calculations where all observed channels are summed while the numbered circles represent the average value for each individual channel. The ratios $R = E^*_{tgt}/E^*_{proj}$ for the corresponding channels are presented in the table below the figure. The error bars reflect the range of variation of the ratio calculated from the FWHM of the excitation energy spectra. The values of R are characteristic of quasi-elastic reactions and do not suggest any evidence for a significant equilibration of energy between target and projectile. That is what one would expect for these reactions with a light projectile and with the requirement of $\Sigma Z = Z_{proj}$.

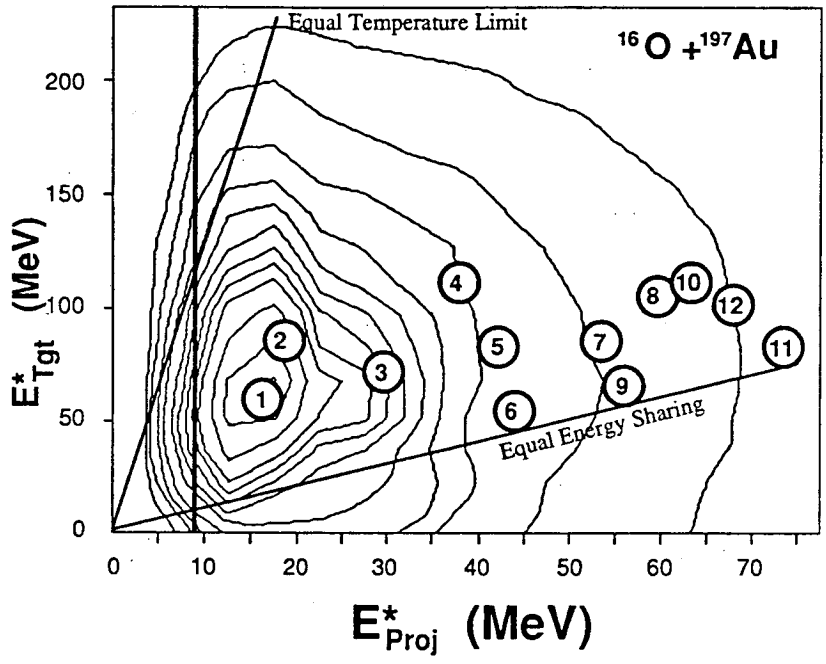

Fig. 5. Excitation energy of the projectile-like nucleus as a function of the target excitation energy. The fully-damped reaction (equal temperature limit) and fast reaction (equal energy sharing) are indicated by the two oblique lines. The vertical line represents the alpha decay threshold of ^{16}O. The numbered open circles show the average value for each channel individually. The numbers relate to the adjacent table. The channels in the table are ordered by decreasing Q value (see also Fig. 3).

^{16}O	Channels	E^*_{tgt}/E^*_{proj}
1	C·He	3.5 ± 0.8
2	N·H	4.5 ± 0.8
3	He·He·He·He	2.5 ± 0.9
4	C·H·H	3.0 ± 0.5
5	B.He.H	1.9 ± 0.7
6	B·Li	1.3 ± 0.5
7	Li·He·He·H	1.6 ± 0.4
8	He·He·He·H·H	1.8 ± 0.4
9	Li·Li·He	1.1 ± 0.4
10	B·H·H·H	1.8 ± 0.5
11	Li·Li·H·H	1.1 ± 0.5
12	Li·He·H·H·H	1.6 ± 0.5

On the average, the ratios get closer to unity as the separation energy increases. The reason for the larger ratios at the lower separation energies is that the projectiles with high excitation energies (and, therefore, with excitation energy ratios closer to unity) decay preferentially into channels with larger numbers of fragments and hence larger separation energies.

It is interesting to note that the increase in average excitation energy in the projectile as one goes from channel 1 to channel 12 (see Fig. 5), is about the same (~50 MeV) as it is in the target. These approximately equal incremental increases in the excitation energies in the projectile and target suggests that the nucleon-nucleon collisions (or exchanges) are becoming an important mechanism for inducing excitation in projectile breakup reactions. Thus, the results shown in Fig. 5 are characteristic of quasi-elastic reactions and do not suggest any evidence for a significant equilibration of energy between target and projectile. This is what one would expect for these reactions with a light projectile and with the requirement that no net charge be transfered.

4. STATISTICAL DECAY CALCULATION

A standard interpretation of projectile breakup consists of factoring the reaction into two independent stages - a fast excitation process followed by decay. The decay may be slow and involve a series of sequential, binary decays. Or the decay may be prompt, implying that the breakup of the projectile occurs while it is still in the vicinity of the target or that its dissociation into three or more fragments occurs more or less simultaneously regardless of location (multifragmentation). It is possible, within this standard interpretation, to analyze the second stage of the reaction by making use of the primary excitation spectrum reconstructed from experiment. We have calculated the yields of the different channels in this way by considering a series of binary splits.

To determine which decays are energetically allowed, the calculation uses a list of binary splits for all nuclei in the mass table. The excess potential U at the saddle point between two nuclei is given by

$$U = E^* + Q - V_b \tag{5}$$

where V_b is the Coulomb barrier. For every split where U is non-negative, the relative probabilities are then calculated from a comparison of the state density at the saddle point and the excitation E*

$$\text{Prob} = \left(\frac{T}{2\pi}\right)\left(\frac{E^*}{U}\right)^2\left(\frac{\exp(2\sqrt{aU})}{\exp(2\sqrt{aE^*})}\right) \tag{6}$$

where T is the temperature[15]. From the excess potential (U), a value equal to twice the temperature goes into kinetic energy (E_k) of the daughter nuclei if $U \geq 2T$; otherwise, all of the remaining energy goes into kinetic energy. The value 2T was chosen because it is the average value for E_k in the Maxwellian, $\text{Prob}(E_k) = E_k \exp(-E_k/T)$. The excess excitation energy ($U-E_k$) is proportionally divided as excitation energy between the two daughter nuclei according to their masses. Some corrections are applied to the proportional division of excitation energy; for instance, protons and neutrons cannot carry excitation energy, and light nuclei that have no states below their lowest threshold for particle decay cannot have an amount of excitation energy less than this threshold. This calculation is similar to one described by Auger, et al.[15], with the exception that ground state masses are used throughout and rotational energy is neglected. A principal feature of this calculation is that, in any binary split, each of the fragments may undergo further decay[10].

The results of this calculation are shown in Fig. 3 and 6. In each case the input was the corresponding experimental primary excitation spectrum (e.g., as in Fig. 4 for ^{16}O). In Fig.3, the individual channels with the same combination of atomic numbers are summed to compare with the data. The calculation compares favorably with experimental results for Q_o values extending down to -30 MeV, which accounts for most of the cross section, but the yields at more negative Q_o values are poorly reproduced, with the calculated values being low by factors of five to twenty. We have also made similar calculations with LILITA (which includes angular momentum and the effects of discrete excited states, but considers the decay of the heavier object only) and obtained qualitatively similar results. Fig. 6 shows the comparison of the observed charge distributions (originated from projectile breakup, $\Sigma Z = Z_{proj}$) with the calculations. The calculations reproduce all the data with an average difference of 35%. It is interesting to point out that the calculations for all projectiles underestimate charges 3 and 5.

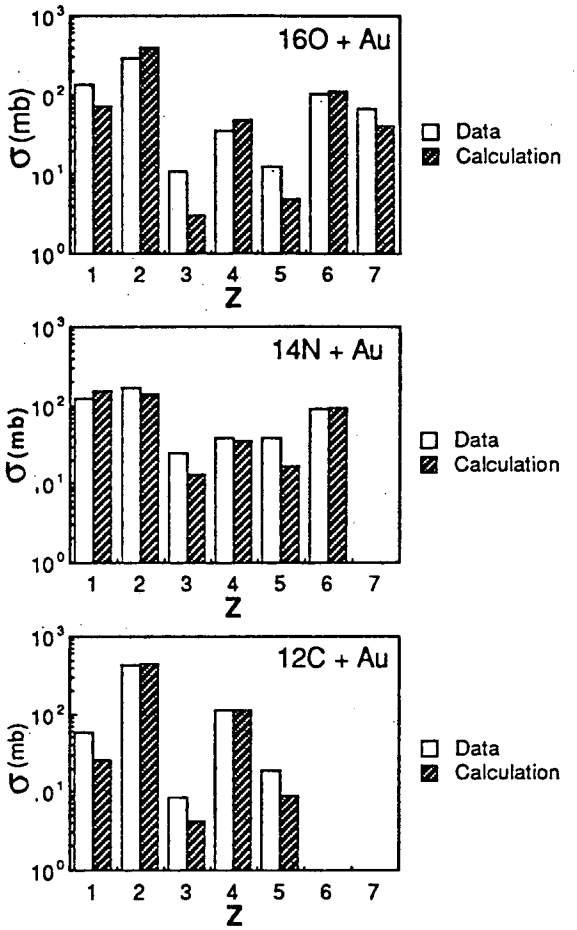

Fig. 6. Charge distributions from the breakup of the projectile-like nucleus for the ^{16}O, ^{14}N and ^{12}C + ^{197}Au systems. The sequential decay calculations are represented by the hatched bars.

5. KINEMATICAL SIGNATURES OF THE BREAKUP PROCESS

We have observed in section 3.3 that the primary system (i.e., the target-like and the projectile-like nuclei) seems to have reached at most a partial equilibrium during the interaction. However, this does not describe how the excited projectile-like nucleus decays after the excitation process. In section 4. we have assumed a multiple sequential decay mechanism to calculate the relative cross sections of the different final channels. This decay mode is known to be dominant in the ≤10 MeV/A energy region[16]. At somewhat higher energies (≥30 MeV/A), the breakup reaction becomes more complex with a higher multiplicity of particles in the exit channel and at relativistic energies, decay by faster process, such as multifragmentation, may contribute to the total yield.

The directional correlations among the particles emitted in a given event contain information on the mechanism of decay of an excited projectile. We have examined the

directional correlations of the fragments emitted in the decay of ^{16}O and compared the calculations of Lopez and Randrup[17] to our results. These authors have developed models for prompt and sequential decay and emphasized the different kinematical signatures associated with these two extreme cases.

We have compared the calculation with several exit channels from the breakup of ^{16}O on a ^{197}Au target. Fig.7 shows the experimental relative angle distribution (6 angles per event) for the four alpha exit channel. The black and open symbols indicate the theoretical folding angle distributions resulting from sequential decay and fragmentation, respectively. A comparison of the calculations with the data indicates that the dominant mode of deexcitation in this case is sequential, where the reaction proceeds as $^{16}O \rightarrow {}^{12}C+\alpha \rightarrow {}^{8}Be(unstable)+\alpha+\alpha \rightarrow \alpha+\alpha+\alpha+\alpha$.

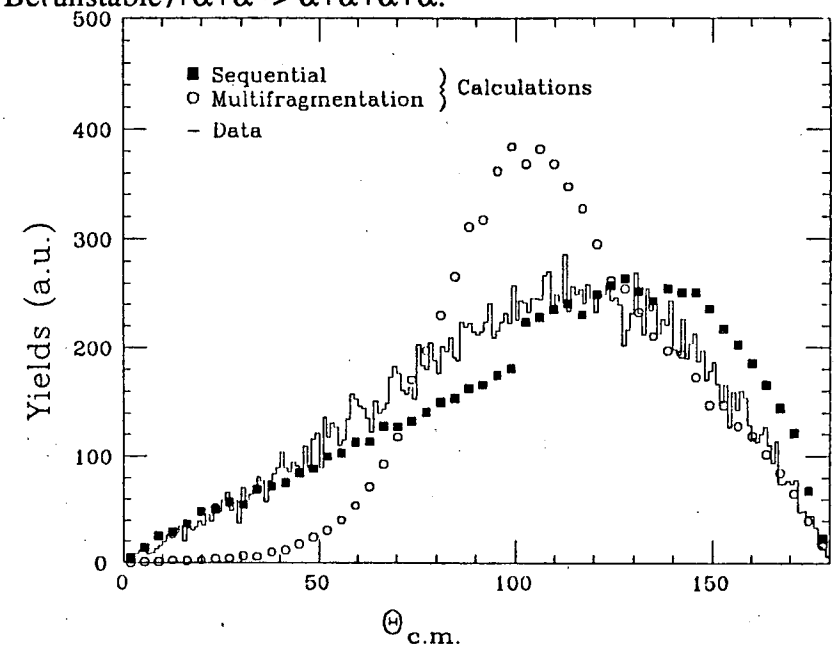

Fig. 7. The relative angle between any pair of alphas from the breakup of $^{16}O+^{197}Au \rightarrow \alpha+\alpha+\alpha+\alpha$ (6 angles per event) in the center of mass of the projectile-like nucleus. The black and open symbols represent the sequential and multifragmentation decay calculations.

A similar comparison can also be made by using the eigenvectors of the kinetic-flow tensor[17,18] to calculate the sphericity and coplanarity of a particular event. Fig.8 shows the coplanarity vs sphericity plot for the 4 α channel. The origin of the plot represents a rod-like shape, while (1,0) is a sphere and (3/4, $\sqrt{3}/4$) is a disk. Fig.8 (c) shows the data and (a) and (b) are the fragmentation and sequential calculations, respectively. The data tend to concentrate along the line delineating the transition from

rod-like to disk-like, characteristic of a sequential decay, unlike the fragmentation calculation which indicates an extension to more spherical distributions. Other channels (such as B+He+H and He+He+He+H+H) have also been studied in the same way with similar results[19].

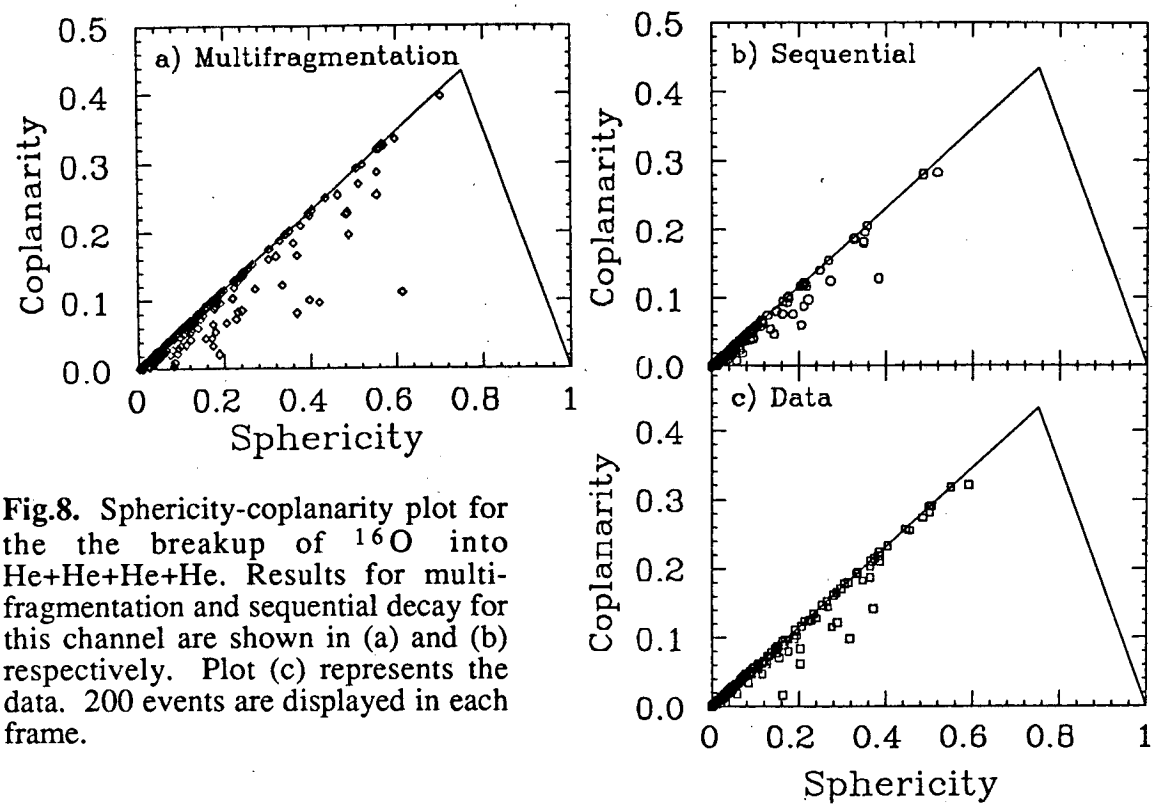

Fig.8. Sphericity-coplanarity plot for the the breakup of ^{16}O into He+He+He+He. Results for multi-fragmentation and sequential decay for this channel are shown in (a) and (b) respectively. Plot (c) represents the data. 200 events are displayed in each frame.

6. SUMMARY

In summary, the cross sections for the breakup of ^{16}O, ^{14}N and ^{12}C projectiles into a large number of exit channels, some having as many as five charged particles, have been measured with an array of 34 plastic scintillators. This has enabled a more global examination of the breakup of the projectile than would be possible with two-particle coincidence experiments. The relative yields of the different channels were observed to correlate approximately with the threshold energy for separation of the projectile into the detected fragments. The excitation spectrum of the primary projectile-like nucleus, deduced from the separation energies and the measured positions and kinetic energies of the individual fragments, peaks at low excitation energies, but also extends to quite high excitation energies (5-6 MeV/A). The sharing of the excitation energy between the

projectile-like nucleus and the target does not indicate any evidence for strong equilibration in the initial stage of the reaction and is thus consistent with a fast excitation process. A multiple sequential decay model for the reaction mechanism can account for the bulk of the cross section and for the trends in the yields but differences between this model and experiment remain. A kinematical study of the data with models for sequential and multifragmentation decay indicates a predominance of multistep sequential emission of nucleons and fragments.

This work was supported by the Director, Office of Energy Research, Division of Nuclear Physics of the office of High Energy and Nuclear Physics of the U.S. Department of Energy under contract DE-AC03-76SF00098.

REFERENCES

1. Dayras R., J. de Phys. Colloque C4 13 (1986).
2. Stokstad R.G., Comments on Nucl. and Part. Phys. 13, 231 (1984).
3. Rae W.D.M. et al., Phys. Lett. B105, 417 (1981) ; Phys. Rev. C30, 158. (1984).
4. Homeyer H., et al., Phys. Rev. C26 , 1335(1982).
5. Pouliot J., et al., Nucl. Inst. and Meth. A270 ,69 (1988).
6. Schmidt H.R., et al., Nucl. Inst. and Meth. A242, 111 (1985).
7. Stokstad R.G., et al., Proc. of the XX Int. Summer School on Nucl.Phys., IOP Publ. Ltd., Poland, Sept. 2-12 (1988).
8. Gomez del Campo J., et al., Phys. Rev. C19, 2170 (1979).
9. Ortiz M.E., et al., Notas de Física, Proceedings of the XI Oaxtepec Symposium on Nuclear Physics, Oaxtepec, Morelos, México, Jan. 4-7 235 (1988) .
10. Knop R. and Stokstad R.G., LBL-Report 26439 (1988).
11. Gazes S., et al., Phys. Letts. B208 194 (1988).
12. Siwek-Wilczynska K., et al., Phys. Rev. C32 1450 (1985); S.Gazes, et al., Phys. Rev C38 712 (1988).
13 P.L. Gonthier, et al., Phys. Rev. C35 (1987) 1946; K. Siwek-Wilczynska, et al., Phys. Rev. C35 (1987) 1316; W. Terlau, et al., Z. Phys. A330 (1988) 303.
14. Sohlbach H. et al., Nucl. Phys. A467 ,349 (1987) .
15. Auger F., et al., Phys. Rev. C35 (1987) 190.
16. Stokstad R.G., Int. Symp. on Nucl. Fission and Heavy-Ion Reduced Reactions, Rochester 1986, Proc. NSRC Series 11, 455 (Harwood, 1987).
17. Lopez J. and Randrup J., Nucl. Phys. A491, 477 (1989); see also Lopez et al, contribution to this meeting.
18. Gyulassy M. et al., LBL-13379 (1981).
19. Harmon A. et al., LBL-26339 (1989).

LAWRENCE BERKELEY LABORATORY
TECHNICAL INFORMATION DEPARTMENT
1 CYCLOTRON ROAD
BERKELEY, CALIFORNIA 94720